Published in final edited form as:
J Neuropathol Exp Neurol. 2012 March ; 71(3): 198–210. doi:10.1097/NEN.0b013e3182482590.

Unmyelinated Axons Show Selective Rostrocaudal Pathology in the Corpus Callosum Following Traumatic Brain Injury

Thomas M. Reeves, PhD, **Terry L. Smith, MS**, **Judy C. Williamson, BA**, and **Linda L. Phillips, PhD**
From Department of Anatomy and Neurobiology, School of Medicine, Virginia Commonwealth University Medical Center, Richmond, Virginia

Abstract

Axonal injury is consistently observed following traumatic brain injury (TBI). Prior research has extensively characterized the post-TBI response in myelinated axons. Despite evidence that unmyelinated axons comprise a numerical majority of cerebral axons, pathological changes in unmyelinated axons following TBI have not been systematically studied. To identify morphological correlates of functional impairment of unmyelinated fibers following TBI, we assessed ultrastructural changes in corpus callosum axons. Adult rats received moderate fluid percussion TBI, which produced diffuse injury with no contusion. Cross-sectional areas of 13,797 unmyelinated, and 3,278 intact myelinated axons were stereologically measured at survival intervals from 3 hours to 15 days post-injury. The mean caliber of unmyelinated axons was significantly reduced at 3 to 7 days, and recovered by 15 days, but the time course of this shrinkage varied among the genu, mid-callosum and splenium. Relatively large unmyelinated axons appeared to be particularly vulnerable. Injury-induced decreases in unmyelinated fiber density were also observed but they were more variable than caliber reductions. By contrast, no significant morphometric changes were observed in myelinated axons. The finding of a preferential vulnerability in unmyelinated axons has implications for current concepts of axonal responses following TBI and for development of specifically targeted therapies.

Keywords

Axonal injury; Corpus callosum; Stereology; Traumatic brain injury; Ultrastructure; Unmyelinated axons

INTRODUCTION

Traumatic brain injury (TBI) is an enduring public health problem, with over 1.5 million new TBIs occurring annually in the United States alone (1). Axonal injury is a concomitant of most TBIs requiring hospitalization. Diffuse axonal injury was recently observed to occur in 72% of patients with moderate or severe TBI and was associated with worse outcome (2). This diffuse pathology is also associated with post-traumatic coma, persistent memory deficits and impaired information processing capacity (3). Despite these serious clinical consequences, fundamental questions remain as to whether all axons are equally susceptible to injury or whether specific populations of axons are selectively vulnerable. Moreover, the

Send correspondence and reprint requests to: Thomas M. Reeves, PhD, Department of Anatomy and Neurobiology, 1217 E. Marshall Street; Room 740, MCV Campus Box 980709, Virginia Commonwealth University, Richmond, VA 23298. Phone: (804) 628-3003; Fax: (804) 828-3276; tmreeves@vcu.edu.

structural and functional changes initiated in axons following TBI are not completely understood.

Accumulating evidence using experimental animal models of TBI suggests that separate populations of axons undergo distinct responses to injury and to treatment with neuroprotective compounds. The longstanding assumption that axon loss is due primarily to shear and tensile forces acting at the moment of injury (4) has been supplanted by an understanding that most injured axons undergo secondary progressive alterations that include cytoskeletal changes, impaired axoplasmic transport and axonal swelling (5–8). On the other hand, observations that some injured axons exhibit neurofilament compaction independently of impaired fast transport (9, 10) and that immunophilin ligand treatment differentially attenuates these abnormalities (11) suggest that within the brain there are subpopulations of axons that undergo different forms of secondary axonal injury. Post-TBI alterations in axonal function also suggest that axon phenotypes are determinants of injury outcome. Axonal excitability, assessed using compound action potentials evoked in the corpus callosum, was more severely suppressed in unmyelinated than in myelinated axons (12, 13). These fiber types exhibit differential degrees of functional protection after treatment with the immunophilin ligands cyclosporin-A (14) and FK506 (15), and the calpain inhibitor MDL-28170 (13). Together, these findings contrast with prevailing concepts of axonal injury being an undifferentiated pathology present in varying degrees but generally affecting axons indiscriminately.

The primary objective of the present study was to investigate TBI-induced ultrastructural changes in axons of the corpus callosum; such changes have been suggested to be the morphological correlates of electrophysiological deficits noted in prior studies (12–17) and they reveal reactive structural alterations specific to the unmyelinated axon population. The majority of prior descriptions of axonal pathology following brain trauma have focused on myelinated axons, but a comprehensive understanding of axonal injury necessitates incorporation of pathological responses specific to unmyelinated fibers.

The experimental TBI model of fluid percussion injury (FPI) in adult rats has been extensively characterized and applied to the study of a wide array of cellular alterations initiated by neurotrauma (18, 19). Our application of FPI at a moderate intensity results in diffuse injury without contusion or hematoma and does not lead to significant Wallerian degeneration. However, the injury does produce functional impairments, including electrophysiological alterations in corpus callosum (12–16) and deficits in spatial cognition without hippocampal cell death (20). Thus, this approach allows the study of nonlethal changes in unmyelinated axons, which comprise the numerical majority of fibers in parasagittal white matter of the cerebrum (21). Because degenerating axons are not salvageable, unmyelinated axons that display time-dependent changes in function and morphology represent potential targets for therapies.

MATERIALS AND METHODS

Animals

The procedures for this study followed all national guidelines for the care and use of experimental animals and the experimental protocol was approved by the Medical College of Virginia Animal Research Committee. Male Sprague-Dawley rats (n = 54) weighing 300 to 350 grams at the start of the study were housed in individual cages in a temperature- (22°C) and humidity- (50% relative) controlled animal facility on a 12-hour light/dark cycle. Rat chow and water were continually available.

FPI

Rats were anesthetized with sodium pentobarbital (100 mg/kg, i.p.) and a 4.8-mm skull craniotomy was prepared over the midline, centered between bregma and lambda. A Leur-Loc syringe hub was cemented with cyanoacrylate to the skull surrounding the craniotomy and dental acrylic was poured around the syringe hub and 2 small screws placed in the skull for implant rigidity. Bacitracin was applied to the incision and the animals were returned to their home cages.

At 24 hours following implantation of the syringe hub, rats were anesthetized with isoflurane (4% in carrier gas of 70% N_2O and 30% O_2), and immediately subjected to moderate central fluid percussion injury, as previously described (22). Briefly, the device consisted of a 60- × 4.5-cm Plexiglas water-filled cylinder, fitted at one end with a piston mounted on O-rings, with the opposite end housing a pressure transducer (Entran Devices, Inc.; EPN-0300A). At the time of injury, the Leur-Loc fitting, filled with saline, was attached to the transducer housing. The injury was produced by a metal pendulum that struck the piston, transiently injecting a small volume of saline into the cranial cavity and briefly deforming the brain tissue (20-ms-pulse duration). The resulting pressure pulse was recorded extracranially by the transducer and expressed in atmospheres of pressure. Injury magnitude was controlled by setting the height from which the pendulum was released. The device was configured to apply a pulse of 2.0 atmospheres (known from prior studies to induce an injury of moderate intensity). Following injury, all animals were promptly ventilated with room air until spontaneous breathing resumed. The duration of suppression of the righting reflex was used as an index of traumatic unconsciousness. Sham-injured controls received the same surgical preparation, anesthesia and connection to the injury device, except that the intracranial pressure pulse was not applied.

Electron Microscopy of Corpus Callosum

Following FPI, rats were randomly assigned to one of the following survival groups: 3 hours (n = 3), 1 day (n = 5), 3 days (n = 4), 7 days (n = 4), 15 days (n = 4). The effects of sham injury were evaluated at 3 hours (n = 2), 1 day (n = 3), 3 days (n = 3), and 7 days (n = 3). At these survival intervals, rats were deeply anesthetized with sodium pentobarbital (60 mg/kg, i.p.) and perfused transcardially with 0.9% saline, followed by mixed aldehyde fixative (4% paraformaldehyde and 0.2% glutaraldehyde) in 0.1M phosphate buffer, pH 7.2. Brains were removed and post-fixed overnight at 4°C. Sagittal sections (40 μm) of corpus callosum were collected in 0.1 M phosphate buffer, and the 4 most medial sections placed in 1% osmium tetroxide (0.1 M sodium cacodylate buffer, pH 7.2, with the addition of 2.5% potassium ferrocyanide) and then processed in Epon resin (EMbed, Electron Microscopy Sciences, Hatfield, PA) prior to flat-embedment on plastic slides. After curing, areas containing callosal regions (genu, midportion, or splenium) were excised, mounted on Epon blocks, and semi-thin (0.5 μm) and ultrathin (silver, 600Å) sections were cut with a Leica EM UC6i ultramicrotome (Leica Microsystems, Wetzlar, Germany). The most medial semi-thin sections were used to generate images of the midsagittal corpus callosum, which were then used to guide subsequent ultrastructural sampling. Mean cross-sectional area of the midsagittal callosum was also used to estimate total number of callosal axons from density measurements. Ultrathin sections were collected on membrane-Formvar-coated slotted grids and observed on a JEOL JEM-1230 electron microscope (JEOL USA, Inc., Peabody, MA) equipped with a Gatan UltraScan 4000SP CCD camera (Gatan, Inc., Pleasanton, CA). Stereological sampling of genu, mid-callosal, and splenium regions was conducted using systematic sampling after a random start (23). At each region, 10 fields of 22.5 μm^2 were digitized at x5,000 magnification, positioned at intervals to span the dorsoventral axis of the callosum (Fig. 1A). Within each field an unbiased counting frame (2.5 μm × 2.0 μm) was constructed, based on the fractionator principle (21, 24). In each frame, axon profiles

meeting an operational definition of 'intact' were outlined using a Wacom PTK-840 graphics tablet (Wacom Technology Corp., Vancouver, WA) to quantify axon density and caliber (fiber cross-sectional area). Experimenter outlined axon profiles while blinded to the injury condition or survival period. Axons were counted as intact if they met 3 criteria: 1) the membrane exhibited a continuous profile; 2) axoplasm contained at least 1 microtubule; and 3) axoplasm showed no degenerative debris. For myelinated axon profiles, 3 contours were outlined and used for cross-sectional area computations: outer myelin border (a); inner myelin border (b); and axolemma (c) (Fig. 1B).

Statistical Analysis

The effects of FPI on axonal cross-sectional area and density were analyzed with ANOVA followed by post hoc analyses using the Dunnett multiple comparison test (SPSS v.11.5). A probability of less than 0.05 was considered significant for all experiments. Results are reported as mean ± SEM.

RESULTS

Prior to the analysis of time-dependent morphological changes associated with FPI, it was essential to ensure that injury levels did not differ significantly among the various survival groups. The fluid percussion device was calibrated to deliver a pressure pulse of 2.0 atmospheres, and the actual measured mean pulse magnitude was 1.98 ± 0.01 atmospheres, averaged across all FPI rats in the study. None of the various survival groups (killed from 3 hours to 15 days) differed significantly from this magnitude ($F_{(4,12)} = 0.407$; $p = 0.800$). A comparison of the duration of suppression of the righting reflex, used as an index of traumatic unconsciousness, provided additional evidence of injury uniformity among survival groups. The overall mean latency to regain the righting reflex for all animals given fluid percussion injury was 5.93 ± 0.16 minutes. None of the survival groups used in the study differed significantly from this overall mean righting latency ($F_{(4,12)} = 0.926$; $p = 0.481$). Among sham rats, length of survival time did not significantly alter any dependent measure in the study; sham rats were pooled into a single (n = 11) group for all statistical analyses.

Callosal Axon Populations in Control (Sham-Injured) Rats

A total of 17,075 axonal profiles (6,659 from sham injured rats, and 10,416 from FPI rats) were digitally traced and cross-sectional areas computed. There were 13,797 unmyelinated and 3,278 myelinated axons measured. Statistical evaluations of post-injury changes to axonal morphology were based on these area measurements. Because previous studies of callosal axon size are reported in terms of fiber diameter, cross-sectional area values were converted to diameters assuming circularity of axonal cylinders. Because the sham injury procedure dissected only the midline scalp and cranium without disturbing the dura or underlying parenchyma, we predicted that axonal morphology in sham operated rats would be equivalent to that in naïve control rats, The frequency distributions of axonal diameters from sham rats for unmyelinated and myelinated fibers combined from all regions observed (genu, mid-callosum and splenium) are shown in Figure 2A. Mean diameters of unmyelinated (0.223 ± 0.002 μm) and myelinated (0.568 ± 0.006 μm) axons corresponded closely to earlier estimates in the corpus callosum of rodents (25–27).

Morphological parameters differed significantly among the callosal regions in sham control rats. The density of unmyelinated axons showed a striking rostrocaudal gradient, i.e. highest in the splenium (mean = $6.2 \times 10^6/mm^2$), falling off by 38.7% in the mid-callosum, and by 54.8% in the genu (Fig. 2B). This regional variation in unmyelinated fiber density was highly significant ($F_{(2,24)} = 19.459$; $p < 0.001$). In contrast, none of the regional estimates of

myelinated axon density differed from an overall mean of $1.1 \times 10^6/mm^2$ ($F_{(2,24)} = 1.627$; $p = 0.218$). Axon diameters in sham control rats also exhibited significant spatial variation with genu fibers being largest for both unmyelinated (mean = 0.26 μm), and myelinated (mean = 0.63 μm) populations. At more caudal locations, mean diameter decreased for both unmyelinated ($F_{(2,24)} = 14.645$; $p < 0.001$) and myelinated ($F_{(2,24)} = 13.580$; $p < 0.001$) axons (Fig. 2B). In comparison to the caliber of genu axons, axon diameters measured at more caudal regions decreased by an average of 17.7% (unmyelinated) and 14.2% (myelinated) (Fig. 2B). Representative micrographs from each region of the callosum in sham-injured rats are shown in Figure 3A–C.

The mean cross-sectional area of the total midsagittal corpus callosum, estimated from the most medial semi-thin sections was 2.97 ± 0.15 mm^2 in sham-injured rats. Based on the above axonal density values and using the present definition of intact axon (continuous membrane profile, at least 1 microtubule, no degenerative debris), the estimated numbers of unmyelinated and myelinated axons in the corpus callosum were $11.55 \pm 0.73 \times 10^6$ and $3.32 \pm 0.17 \times 10^6$, respectively. This yields a total of about 14.87×10^6 axons in the corpus callosum of adult male Sprague-Dawley rats, of which 77.7% are unmyelinated. These results are comparable to whole-callosum estimates provided in an early study that reported a cross-sectional area of 2.6 mm^2, and a total of 12×10^6 axons (25). Those authors used an essentially identical sampling scheme in rats at 60 d of age. Similarly, they reported that 80.8% of axons in the corpus callosum are unmyelinated (25), which is in close agreement with our estimates.

Effects of FPI on Callosal Axon Caliber and Density

The FPI used induces diffuse injury that results in electrophysiological (12, 14, 15) and behavioral (20) deficits with little or no cell death and only modest axonal degeneration. No areas of parenchyma contusion were observed during dissection. The ultrastructural appearance of injured corpus callosum was usually quite similar to that from control rats with the exception that most injured cases exhibited more astrocyte profiles, consistent with a post-injury activation of astroglia. Even though quantitative analyses revealed significant morphometric changes to axonal dimensions at 3 days post-injury, there was a qualitative similarity to controls in the general fiber architecture and the rostral-to-caudal increase in unmyelinated axon density in the injured rats at that time point (Fig. 3D–F).

Quantitative assessment of injury-related changes to cross-sectional area and density of axons was done in 2 phases. First, data from all regions were aggregated together to estimate the generalized effect of fluid percussion on the corpus callosum as a whole. Then, separate analyses that focused on TBI-related changes within each callosal region were done.

Analyses of axonal cross-sectional area based on combined data from all callosal regions, revealed a transient injury-induced decrease in unmyelinated axon area; this effect reached significance at 3 days (20.0% below sham levels; $p < 0.05$) and 7 days (22.8% below sham levels; $p < 0.05$) following injury. However, by day 15 post-injury, mean unmyelinated axon area was not different from that in controls (Fig. 4A). Figure 4 (and similar figures) depict post-injury values normalized to sham control means. Supplemental Digital Content 1 (http://links.lww.com/NEN/A315) contains corresponding tables of all analytic measures (mean ± SEM) in physical units (μm^2 for cross-sectional area and number per mm^2 [$\times 10^6$] for density) tabulated for each time point at each region and containing whole-callosum estimates aggregated from the regional data.

Examination of time-dependent changes in mean cross-sectional areas of myelinated axons suggested initial post-injury swelling at 3 hours and 1 day, but these increases did not reach significance (Fig. 4A). Myelinated fiber caliber overall did not significantly differ from

sham control levels at any post-injury time point ($F_{(5,25)} = 0.639$; $p = 0.672$). Area measures, which included the axon plus myelin (contour 'a' in Fig. 1), also did not significantly vary from sham levels at any time point after injury ($F_{(5,25)} = 0.592$; $p = 0.706$).

The ratio of the inner axonal diameter to the total outer diameter, commonly referred to as the "g-ratio," has been widely employed as a structural index of optimal axonal myelination since the historical work of Rushton (28). The g-ratio has been reported to change in some models of experimental neurotrauma, such as myelin thinning following a compressive spinal cord injury (29). In the present group of sham-injured rats, the mean g-ratio was 0.708 ± 0.008, which approximates the optimal ratio for conduction velocity predicted by computer simulation (30). The g-ratio was not significantly altered by FPI at any callosal regions or for the callosum as a whole.

In comparison to the FPI-induced decline in mean cross-sectional area of unmyelinated axons, post-injury changes in the density of intact callosal fibers were more variable. The experiment was designed to detect numerical losses of fibers which met the operational definition of "intact," possibly reflecting sublethal cytoskeletal, organelle, or membranous alterations. The mean density of callosal unmyelinated axons based on combined data from all callosal regions was below the sham control level at all post-injury time points. This reduction did not reach significance in a statistical design with survival interval as a factor, and which could detect time-dependent changes in density ($F_{(5,24)} = 1.182$; $p = 0.347$) (Fig. 4B). Nevertheless, several aspects of Figure 4B suggest that the density of unmyelinated fibers was influenced by FPI to some degree as follows: 1) the mean density values were consistently below sham levels; 2) both density and area changes were maximal at 7 days; and 3) both processes trended towards recovery between 7 to 15 days. A post-hoc analysis that pooled all post-injury time points did show significant injury-related reduction in unmyelinated fiber density ($F_{(1,28)} = 5.855$; $p = 0.022$). Using similar pooling for regions showed that the greatest decrease in unmyelinated axon density was a 27.16 ± 7.13% decrease in the splenium ($p < 0.05$), followed by a 23.67 ± 6.23% decrease in mid-callosum ($p < 0.05$); a 4.76 ± 7.72% density change in the genu was not significant. The density of myelinated axons was not significantly altered by the fluid percussion injury ($F_{(5,25)} = 0.805$; $p = 0.557$) (Fig. 4B). Consistent with the modest effect of injury on axonal density, FPI did not significantly alter the dimensions of the total corpus callosum structure observed at the midline in semi-thin sections. The mean cross-sectional area of the total midsagittal corpus callosum computed from all FPI rats was 2.84 ± 0.16 mm^2; none of the survival groups differed from the area of the callosum observed in sham rats (2.97 ± 0.15 mm^2) ($F_{(5,21)} = 0.521$; $p = 0.758$).

Following TBI, unmyelinated axons exhibited distinct abnormalities related to their decreased density. In some cases, there were isolated unmyelinated profiles that displayed membrane discontinuities or cytoplasmic abnormalities that prevented them from being scored as intact. This often took the form of atrophic changes where the axoplasm appeared to constrict, producing empty membranous folds and aberrant spaces in the adjacent extracellular compartment (Fig. 5A). In other cases, there were clusters of unmyelinated axons with degenerative changes affecting multiple fiber profiles. These groups of axons typically displayed axolemmal deterioration with untraceable membranes that prevented their designation as intact (Fig. 5B). Additionally, there was an apparent selective vulnerability of relatively large axons, which often demonstrated axoplasmic constriction and membrane folding. These malformed large axons were sometimes observed within fields of intact small unmyelinated axons (Fig. 5C).

Analyses of unmyelinated axons within each callosal region revealed an FPI-induced reduction in fiber caliber that initially affected the splenium at day 1 and then progressed

rostrally to impact the mid-callosal region at day 3, and finally the genu at day 7 post-injury (Fig. 6). At these time points, statistically significant peak decreases in cross-sectional axon area of −30.8%, −30.0%, and −26.4% were observed for the splenium, mid-callosum, and genu, respectively (Fig. 6). None of the callosal regions exhibited significant alterations in myelinated axon caliber or density (Supplemental Digital Content 1).

It is possible that post-injury changes in cross-sectional area did not affect all unmyelinated axons uniformly, and this was also examined quantitatively. For example, relatively large unmyelinated axons may have been injured to a different extent from smaller fibers. As an initial approach to this issue, quartile values were computed for the unmyelinated axon diameters in sham injured rats, which were then used to assess injury-induced changes in the distribution of axon diameters in each callosal region (Fig. 7). Each panel establishes the quartiles for sham controls (first column) for a region, and columns to the right show how FPI altered the distribution of fiber diameters relative to the sham baseline. For example, 25.0% of the 2,603 axons in the splenium of sham rats had diameters less than or equal to 0.14 μm, whereas among 937 splenial axons measured at 1 day post-injury, 43.1% of fibers had diameters ≤0.14 μm (Fig. 7A). The increase in the proportion of fibers with small (≤0.14 μm) diameters was accompanied by decreases in the proportion of larger fibers, particularly fibers in the top quartile (≥0.27 μm), which decreased to 14.8% of unmyelinated axons measured in the splenium at 1 day after FPI. It is notable that the greatest increase in the lowest quartile occurred at day 1 post-injury in the splenium, at 3 days in the mid-callosum, and at 7 days in the genu (open arrows) (Fig. 7). These survival intervals match the time of greatest decrease in the mean cross-section areas (Fig. 6). The quartile analysis was based on axon area measurements, as well as fiber density, the latter of which was more variable after injury. This was likely the reason that significance tests for the data of Figure 7 showed that post-injury increases in the lowest quartile were only significant for the splenium ($F_{(5,20)} = 3.773$; $p = 0.014$). Finally, Figure 7 indicates that, for each region, the time of greatest increase in lowest quartile fibers was followed by a recovery to a quartile pattern very similar to that of sham controls. This is in agreement with the data in Figure 6, and probably reflects a time-dependent post-injury axonal shrinkage, followed by morphological recovery. However, this recovery may also reflect a delayed loss of lowest-quartile fibers that no longer met the operational definition of ‘intact’. Thus, it is conceivable that some larger axons underwent shrinkage, thereby increasing the numbers counted as lowest-quartile fibers. These axons might have further continued to deteriorate (in membrane or microtubules) to a degree that they could not be counted as intact. Preferential loss of these lowest-quartile axons would tend to re-balance the distribution of fiber calibers; the quartile breakdown would then tend to more resemble the sham control pattern.

The preceding analysis revealed a time-dependent process wherein the proportion of unmyelinated fibers in the highest diameter quartile transiently decreased and the smallest quartile membership increased; this effect progressed in a caudal-to-rostral pattern. Because relatively large unmyelinated axons may play a pivotal role in these changes, the largest quartile was further analyzed in detail by examining the time courses of post-TBI changes in the largest 10%, 5%, and 1% of fibers (using cutoff values based on the 90th, 95th, and 99th percentile of the sham control axons). When this analysis was conducted on the whole corpus callosum, averaging across all subregions, the results suggested some tendency for the largest axons to be at greater risk after TBI. The numbers of intact axons in the top 25%, 10%, and 5% of fiber diameters were generally below control values on post-TBI day 1 and day 3, although this only reached significance for the 10% subpopulation at day 7 ($p < 0.05$) (Fig. 8A). In contrast, the largest 1% was significantly less numerous at day 1 and day 3 ($p < 0.05$); this reduction remained significant even at day 15 ($p < 0.05$), when the other fiber categories had converged toward control values (Fig. 8A). Importantly, axons in the largest

1% category were so sparse, following injury, that a time course could only be established for the whole callosum. In sham control rats there was an average of only 5.4 fibers with diameters in the top 1% summed across all regions, compared to a mean of 3.4 fibers in injured rats. A detailed time course at the regional level was not possible because of the small numbers of axons in the top 1% diameter range for at least one region in the injured rats: 80% of injured rats had no fibers in the top 1% in the genu (although this decrease was less severe in injured splenium and middle callosum, where 40% of injured rats had no fibers in the top 1%). Figure 8B summarizes post-injury changes in the top 25%, 10%, and 5% categories, confirming the temporal gradient of significant mean diameter decrease in the splenium at 1 day, and progressing to caliber loss in the genu at 7 days. This time course reflected significant declines in fibers in the top 25% class but that reductions in the 5% category also reached significance in the genu.

DISCUSSION

The findings of this study indicate that for the specific injury conditions of moderate central FPI, unmyelinated axons undergo responses that are quite distinct from those of myelinated axons. The midline FPI model was selected for this study to match prior experiments showing functional impairments (12, 13, 20), and to explore nonlethal axonal changes in a white matter environment with minimal fiber degeneration. Although regarded as a moderate intensity injury, the 2.0 atmospheres midline FPI used here elicits less axonal injury and degeneration in the cerebrum than most alternative animal models of TBI, including lateral FPI, controlled cortical impact and impact-acceleration (31, 32). The microscopic examination in the present study did not demonstrate significant degrees of axonal swelling, bulb formation or Wallerian degeneration, which are reliably elicited in brainstem white matter tracts following impact acceleration injury in adult rats (10, 11, 33–36). Indeed, the FPI-induced morphological changes in this study were relatively modest and required a quantitative stereological assessment for their characterization. These results may, therefore, have implications for the clinical condition of mild TBI, which often goes unreported and has been estimated to be approximately 22 times more prevalent than severe TBI (37). We observed post-TBI time-dependent cellular changes that are not necessarily lethal but may contribute to functional impairment that is concomitant with white matter subjected to mild TBI.

A key objective of the study was to establish the fiber composition of the corpus callosum in sham-injured rats as a valid estimate of the normal condition and to provide a reliable baseline against which to evaluate the effects of injury. This was warranted in view of variability among published reports regarding the percentage of unmyelinated axons in the rodent corpus callosum. Earlier studies of axon types in the rodent splenium estimated that about 45% of fibers were unmyelinated (38), but more recent studies have consistently estimated the proportion to be approximately 88% (25, 39, 40); our present estimate of 84% is in line with these reports. The consensus among the more recent estimates is likely due to sampling strategies that systematically cover the dorsal-to-ventral extent of the callosum. Among these prior studies, only Gravel et al (25) implemented a sampling methodology that was essentially equivalent to the present approach, including estimates at genu, mid-callosum, and splenium. Averaging across all regions, those authors estimated that 81% of corpus callosum axons were unmyelinated, which corresponds closely to our estimate of 78%.

Almost all previous reports of TBI-induced changes in axon caliber have referred to focal axon swellings in myelinated axons that are usually associated with cytoskeletal degradation and resultant impairments of axoplasmic transport. Early events include focal axolemmal perturbations that are probably mechanically induced during the injury and are associated

with aberrant permeability (41, 42). Subsequently, microtubule loss and altered neurofilaments lead to focal swellings in myelinated axons (33, 43, 44). These changes are observed in white matter that is subjected to greater injury forces than applied in the present study. We hypothesize that changes in the unmyelinated axon population, including the reduction in area observed in the current study, likely coexist with the abnormalities of myelinated axons in models of more severe TBI. Even within myelinated axons, a type of axonal shrinkage that takes the form of focal decreases in internodal axonal diameter has been described (41). In the current study, caliber measurements were based on sagittal sections that present axons in cross-section; these results do not address whether the observed changes in area occur at focal points along the unmyelinated axons or are expressed uniformly along the fiber length.

The finding of distinctive reactive changes in unmyelinated fibers adds to growing evidence that traumatic axonal injury has more heterogeneous features than previously considered. It is becoming clear that many injured axons do not exhibit the sequence of changes observed in myelinated axons. For example, axons showing cytoskeletal disruption do not invariably progress to swelling (45), and neurofilament compaction is not invariably associated with impaired axoplasmic transport (9, 10). One factor underlying such divergence of reactive changes may be axon heterogeneity, i.e. there likely are subpopulations of fibers with distinct molecular or structural properties. It is likely that myelinated and unmyelinated fibers are distinctive in more ways than diameter and/or the presence of myelin. Indeed, freeze fracture electron microscopy study indicated that axolemma in unmyelinated axons differs from that in myelinated axons at the macromolecular level (46). These authors found that P-face intramembranous particles were more numerous in the internodal myelinated axolemma than in unmyelinated axolemma. Intrinsic differences in membrane constituents may influence fiber vulnerability. Indeed, the pattern and time course of structural changes that we observed in callosal fibers corresponds in several respects to suppression of compound action potentials (CAPs) previously reported using the same FPI model (12). Post-injury reductions in evoked response amplitude were larger for unmyelinated, than for myelinated, CAPs. CAPs evoked through unmyelinated fibers were significantly suppressed at all time points recorded (3 hours – 7 days), whereas FPI-induced impairments to the myelinated CAPs were more transient and had recovered to control levels by 7 days post-injury. Previous CAPs were acquired in the mid-callosal region (12, 15); more detailed analyses of CAP impairments at genu, mid-callosal and splenial regions are now in progress in our laboratory.

Differences in size and the presence or absence of myelin are likely to be primary factors in the contrasting injury responses of the axon types. Axons are the subcellular compartment with the highest membrane-to-cytoplasm ratio, which likely places them at risk to membrane-targeting pathomechanisms of TBI, including lipid peroxidation (47, 48), rapid proteolysis of voltage-gated sodium channels (49, 50), and more protracted proteolytic events attacking submembrane ankyrin (51) and spectrin (52–54). We hypothesize that, because of their higher average axolemma-to-axoplasm ratio, unmyelinated axons are at a greater risk to these processes than myelinated axons. This relationship is illustrated in Figure 9A, which models axons as uniform cylinders of arbitrary length and plots the present measured values of mean axon diameter on the curve relating surface-to-volume ratio to diameter. This demonstrates that the mean diameter of unmyelinated axons (0.22 μm) is approximately 60% smaller than the mean myelinated diameter (0.57 μm); this corresponds to a 160% increase in the surface-to-volume ratio. Intracellular calcium loading, a key TBI pathomechanism, may especially challenge small axons with less cytoplasmic volume and calcium buffering/sequestration capacity, which is known to be critical in white matter injury (55). These factors might contribute to a more significant injury response in unmyelinated axons as a class, as compared to the relatively mild response in myelinated

fibers, which are typically much larger. Whereas it remains possible that unmyelinated axons of all sizes underwent some degree of post-injury shrinkage, the present results (Figs. 5C, 7, 8) suggest that within the population of unmyelinated fibers, comparatively large diameter may comprise an additional risk factor.

Irrespective of axonal size, the presence of myelin itself, which provides physical support and influences fiber subtype vulnerability may account for some degree of axonal protection. In contrast, unmyelinated axolemma is extensively exposed to a post-traumatic extracellular environment with aberrant ionic composition (56), reactive matrix metalloproteinases (57, 58), and infiltrating peripheral factors after blood-brain barrier disruption (51) (Fig. 9B). The intimate exposure of unmyelinated axolemma to the extracellular compartment could also underlie differential responses to drug treatments, such as a greater functional protection for unmyelinated, over myelinated, axons conferred by a calpain inhibitor (13).

Assessments of fiber density in this study also confirmed rostrocaudal heterogeneity of axonal composition, as previously described (25) and cross-sectional area measurements provided, for the first time, a stereological quantification of regional variation in mean diameter for both fiber types. The effects of FPI were regionally specific, with reduced unmyelinated size appearing first in the splenium and then progressing to more anterior zones. This injury sequence may reflect the intrinsic rostrocaudal gradient in unmyelinated axon density. This result may also in part reflect the proximity of the FPI location overlying the mid-callosum and splenium (Fig. 1A), which showed axonal shrinkage prior to the genu. However, it would be difficult to attribute the different latencies to maximum shrinkage (1 day for splenium and 3 days for mid-callosum) to different distance from the FPI location. In the cuprizone demyelination, pathological changes were expressed in a rostrocaudal sequence (59, 60), consistent with the concept that properties intrinsic to specific callosal regions may determine the timing and magnitude of pathological alterations.

In summary, the present results provide evidence that moderate FPI applied to the midline of adult rats induced selective morphological changes in unmyelinated axons of the corpus callosum. A time-dependent reduction in mean axonal caliber, and its subsequent recovery, was highly significant. Reductions in unmyelinated axon density were also detected but were variable. Our findings have implications for current concepts of axonal injury that have tended to focus on pathology in larger myelinated axons. The diminutive size of unmyelinated fibers presents challenges to any monitoring of these structures in clinical, and even experimental, applications but a comprehensive model of axonal injury must account for distinctive alterations that affect the numerical majority of cerebral white matter axons. Injury-induced reductions in average axonal size would likely reduce the mean conduction velocities in these fibers and possibly contribute to the cognitive and memory impairments that are frequently observed after TBI. Although quantitative magnetic resonance imaging has confirmed TBI-induced shrinkage of white matter area (61, 62), the basis of these changes has not been identified at the cellular level. Fiber atrophy, perhaps related to the axonal changes described here may contribute to post-traumatic the white matter shrinkage observed in patients.

Supplementary Material

Refer to Web version on PubMed Central for supplementary material.

Acknowledgments

Supported by the National Institutes of Health (grants NS057758, NS056247, NS047463) and Virginia Commonwealth Neurotrauma Initiative 07-302F. Microscopy was performed at VCU, Department of Anatomy and

Neurobiology Microscopy Facility, which is supported, in part, with funding from NIH-NINDS Center Core Grant NS047463.

The authors wish to thank Lesley Harris, Raiford Black, and Nancy Lee for their excellent technical assistance in this study.

References

1. Rutland-Brown W, Langlois JA, Thomas KE, et al. Incidence of traumatic brain injury in the United States, 2003. J Head Trauma Rehabil. 2006; 21:544–8. [PubMed: 17122685]
2. Skandsen T, Kvistad KA, Solheim O, et al. Prevalence and impact of diffuse axonal injury in patients with moderate and severe head injury: a cohort study of early magnetic resonance imaging findings and 1-year outcome. J Neurosurg. 2010; 113:556–63. [PubMed: 19852541]
3. Meythaler JM, Peduzzi JD, Eleftheriou E, et al. Current concepts: diffuse axonal injury-associated traumatic brain injury. Arch Phys Med Rehabil. 2001; 82:1461–71. [PubMed: 11588754]
4. Strich SJ. Shearing of nerve fibers as a cause of brain damage due to head injury: a pathological study of twenty cases. Lancet. 1961; 2:443–8.
5. Maxwell WL, Povlishock JT, Graham DL. A mechanistic analysis of nondisruptive axonal injury: a review. J Neurotrauma. 1997; 14:419–40. [PubMed: 9257661]
6. Povlishock JT, Christman CW. The pathobiology of traumatically induced axonal injury in animals and humans: a review of current thoughts. J Neurotrauma. 1995; 12:555–64. [PubMed: 8683606]
7. Saatman KE, Graham DI, McIntosh TK. The neuronal cytoskeleton is at risk after mild and moderate brain injury. J Neurotrauma. 1998; 15:1047–58. [PubMed: 9872461]
8. Smith DH, Chen XH, Nonaka M, et al. Accumulation of amyloid beta and tau and the formation of neurofilament inclusions following diffuse brain injury in the pig. J Neuropathol Exp Neurol. 1998; 58:982–92. [PubMed: 10499440]
9. DiLeonardi AM, Huh HW, Raghupathi R. Impaired axonal transport and neurofilament compaction occur in separate populations of injured axons following diffuse brain injury in the immature rat. Brain Res. 2009; 1263:174–82. [PubMed: 19368848]
10. Stone JR, Singleton RH, Povlishock JT. Intra-axonal neurofilament compaction does not evoke local axonal swelling in all traumatically injured axons. Exp Neurol. 2001; 172:320–31. [PubMed: 11716556]
11. Marmarou CR, Povlishock JT. Administration of the immunophilin ligand FK506 differentially attenuates neurofilament compaction and impaired axonal transport in injured axons following diffuse traumatic brain injury. Exp Neurol. 2006; 197:353–62. [PubMed: 16297913]
12. Reeves TM, Phillips LL, Povlishock JT. Myelinated and unmyelinated axons of the corpus callosum differ in vulnerability and functional recovery following traumatic brain injury. Exp Neurol. 2005; 196:126–39. [PubMed: 16109409]
13. Ai J, Liu E, Wang J, et al. Calpain inhibitor MDL-28170 reduces the functional and structural deterioration of corpus callosum following fluid percussion injury. J Neurotrauma. 2007; 24:960–78. [PubMed: 17600513]
14. Colley BS, Phillips LL, Reeves TM. The effects of cyclosporin-A on axonal conduction deficits following traumatic brain injury in adult rats. Exp Neurol. 2010; 224:241–51. [PubMed: 20362574]
15. Reeves TM, Phillips LL, Povlishock JT. Preferential neuroprotective effect of tacrolimus (FK506) on unmyelinated axons following traumatic brain injury. Brain Res. 2007; 1154:225–36. [PubMed: 17481596]
16. Baker AJ, Phan N, Moulton RJ, et al. Attenuation of the electrophysiological function of the corpus callosum after fluid percussion injury in the rat. J Neurotrauma. 2002; 19:587–99. [PubMed: 12042094]
17. Creed JA, DiLeonardi AM, Fox DP, et al. Concussive brain trauma in the mouse results in acute cognitive deficits and sustained impairment of axonal function. J Neurotrauma. 2011; 28:547–63. [PubMed: 21299360]
18. Thompson HJ, Lifshitz J, Marklund N, et al. Lateral fluid percussion brain injury: a 15-year review and evaluation. J Neurotrauma. 2005; 22:42–75. [PubMed: 15665602]

19. O'Connor WT, Smyth A, Gilchrist MD. Animal models of traumatic brain injury: a critical evaluation. Pharmacol Ther. 2011; 130:106–13. [PubMed: 21256863]
20. Lyeth BG, Jenkins LW, Hamm RJ, et al. Prolonged memory impairment in the absence of hippocampal cell death following traumatic brain injury in the rat. Brain Res. 1990; 526:249–58. [PubMed: 2257484]
21. Partadiredja G, Miller R, Oorschot DE. The number, size, and type of axons in rat subcortical white matter on left and right sides: a stereological, ultrastructural study. J Neurocytol. 2003; 32:1165–79. [PubMed: 15044847]
22. Dixon CE, Lyeth BG, Povlishock JT, et al. A fluid percussion model of experimental brain injury in the rat. J Neurosurg. 1987; 67:110–19. [PubMed: 3598659]
23. Mouton, PR. Principles and practices of unbiased stereology: An introduction for bioscientists. Baltimore, MD: Johns Hopkins Univ. Press; 2002.
24. Larsen JO. Stereology of nerve cross sections. J Neurosci Meth. 1998; 85:107–18.
25. Gravel C, Sasseville R, Hawkes R. Maturation of the corpus callosum of the rat: II. Influence of thyroid hormones on the number and maturation of axons. J Comp Neurol. 1990; 291:147–61. [PubMed: 2298928]
26. Sturrock RR. Myelination of the mouse corpus callosum. Neuropath Applied Neurobiol. 1980; 6:415–20.
27. Waxman SG, Swadlow HA. Ultrastructure of visual callosal axons in the rabbit. Exp Neurol. 1976; 53:115–27. [PubMed: 964332]
28. Rushton WA. A theory of the effects of fibre size in medullated nerve. J Physiol. 1951; 115:101–22. [PubMed: 14889433]
29. Nashmi R, Fehlings MG. Changes in axonal physiology and morphology after chronic compressive injury of the thoracic spinal cord. Neuroscience. 2001; 104:235–51. [PubMed: 11311546]
30. Smith RS, Koles ZJ. Myelinated nerve fibers: computed effect of myelin thickness on conduction velocity. Am J Physiol. 1970; 219:1256–8. [PubMed: 5473105]
31. Gennarelli TA. Animate models of human head injury. J Neurotrauma. 1994; 11:357–68. [PubMed: 7837277]
32. Povlishock JT, Hayes RL, Michel ME, et al. Workshop on animal models of traumatic brain injury. J Neurotrauma. 1994; 11:723–32. [PubMed: 7723071]
33. Povlishock JT, Marmarou A, McIntosh T, et al. Impact acceleration injury in the rat: Evidence for focal axolemma change and related neurofilament sidearm alteration. J Neuropathol Exp Neurol. 1997; 56:347–59. [PubMed: 9100665]
34. Okonkwo DO, Buki A, Siman R, Povlishock JT. Cyclosporin A limits calcium-induced axonal damage following traumatic brain injury. Neuroreport. 1999; 10:353–8. [PubMed: 10203334]
35. Buki A, Okonkwo DO, Povlishock JT. Post-injury cyclosporin A administration limits axonal damage and disconnection in traumatic brain injury. J Neurotrauma. 1999; 58:365–75.
36. Singleton RH, Stone JR, Okonkwo DO, et al. The immunophilin ligand FK506 attenuates axonal injury in an impact-acceleration model of traumatic brain injury. J Neurotrauma. 2001; 18:607–14. [PubMed: 11437083]
37. Tagliaferri F, Compagnone C, Korsic M, et al. A systematic review of brain injury epidemiology in Europe. Acta Neurochir (Wien). 2006; 148:255–68. [PubMed: 16311842]
38. Seggie J, Berry M. Ontogeny of interhemispheric evoked potentials in the rat: significance of myelination of the corpus callosum. Exp Neurol. 1972; 35:215–32. [PubMed: 5030850]
39. Juraska JM, Kopcik JR. Sex and environmental influences on the size and ultrastructure of the rat corpus callosum. Brain Res. 1988; 450:1–8. [PubMed: 3401704]
40. Kim JHY, Ellman A, Juraska JM. A re-examination of sex differences in axon density and number in the splenium of the rat corpus callosum. Brain Res. 1996; 740:47–56. [PubMed: 8973797]
41. Pettus EH, Christman CW, Giebel ML, et al. Traumatically induced altered membrane permeability: its relationship to traumatically induced reactive axonal change. J Neurotrauma. 1994; 11:507–22. [PubMed: 7861444]
42. Maxwell WL, McCreath BJ, Graham DI, et al. Cytochemical evidence for redistribution of membrane pump calcium-ATPase and ecto-Ca-ATPase activity, and calcium influx in myelinated

nerve fibers of the optic nerve after stretch injury. J Neurocytol. 1995; 24:925–42. [PubMed: 8719820]

43. Jafari SS, Maxwell WL, Neilson M, et al. Axonal cytoskeletal changes after nondisruptive axonal injury. J Neurocytol. 1997; 26:207–21. [PubMed: 9192287]
44. Povlishock JT. Traumatically induced axonal injury: pathogenesis and pathobiological implications. Brain Pathol. 1992; 2:1–12. [PubMed: 1341941]
45. Marmarou CR, Walker S, Davis CL, et al. Quantitative analysis of the relationship between intra-axonal neurofilament compaction and impaired axonal transport following diffuse traumatic brain injury. J Neurotrauma. 2005; 22:1066–80. [PubMed: 16238484]
46. Waxman SG, Black JA. Unmyelinated and myelinated axon membrane from rat corpus callosum: differences in macromolecular structure. Brain Res. 1988; 453:337–43. [PubMed: 3401771]
47. Evans PH. Free radicals in brain metabolism and pathology. Br Med Bull. 1993; 49:577–87. [PubMed: 8221024]
48. Xiong Y, Rabchevsky AG, Hall ED. Role of peroxynitrite in secondary oxidative damage after spinal cord injury. J Neurochem. 2007; 100:639–49. [PubMed: 17181549]
49. Iwata A, Stys PK, Wolf JA, et al. Traumatic axonal injury induces proteolytic cleavage of the voltage-gated sodium channels modulated by tetrodotoxin and protease inhibitors. J Neurosci. 2004; 24:4605–13. [PubMed: 15140932]
50. von Reyn CR, Spaethling JM, Mesfin MN, et al. Calpain mediates proteolysis of the voltage-gated sodium channel alpha-subunit. J Neurosci. 2009; 29:10350–6. [PubMed: 19692609]
51. Reeves TM, Greer JE, Vanderveer AS, et al. Proteolysis of submembrane cytoskeletal proteins ankyrin-G and αII spectrin following diffuse brain injury: a role in white matter vulnerability at nodes of Ranvier. Brain Pathol. 2010; 20:1055–68. [PubMed: 20557305]
52. Hall ED, Sullivan PG, Gibson TR, et al. Spatial and temporal characteristics of neurodegeneration after controlled cortical impact in nice: more than a focal brain injury. J Neurotrauma. 2005; 22:252–65. [PubMed: 15716631]
53. Saatman KE, Abai B, Grosvenor A, et al. Traumatic axonal injury results in biphasic calpain activation and retrograde transport impairment in mice. J Cereb Blood Flow Metab. 2003; 23:34–42. [PubMed: 12500089]
54. Saatman KE, Creed J, Raghupathi R. Calpain as a therapeutic target in traumatic brain injury. Neurotherapeutics. 2010; 7:31–42. [PubMed: 20129495]
55. Stys PK. White matter injury mechanisms. Cur Mol Med. 2004; 4:113–30.
56. Hovda DA, Becker DP, Katayama Y. Secondary injury and acidosis. J Neurotrauma. 1992; 9 (Suppl 1):S47–60. [PubMed: 1588632]
57. Kim HJ, Fillmore HL, Reeves TM, et al. Elevation of hippocampal MMP-3 expression and activity during trauma-induced synaptogenesis. Exp Neurol. 2005; 192:60–72. [PubMed: 15698619]
58. Falo MC, Fillmore HL, Reeves TM, et al. (2006) Matrix metalloproteinase-3 expression profile differentiates adaptive and maladaptive synaptic plasticity induced by traumatic brain injury. J Neurosci Res. 2006; 84:768–81. [PubMed: 16862547]
59. Wu QZ, Yang Q, Cate HS, et al. MRI identification of the rostral-caudal pattern of pathology within the corpus callosum in the cuprizone mouse model. J Magn Reson Imaging. 2008; 27:446–53. [PubMed: 17968901]
60. Xie M, Tobin JE, Budde MD, et al. Rostrocaudal analysis of corpus callosum demyelination and axon damage across disease stages refines diffusion tensor imaging correlations with pathological features. J Neuropathol Exp Neurol. 2010; 69:704–16. [PubMed: 20535036]
61. Bigler ED, Anderson CV, Blatter DD. Temporal lobe morphology in normal aging and traumatic brain injury. AJNR Am J Neuroradiol. 2002; 23:255–66. [PubMed: 11847051]
62. Spanos GK, Wilde EA, Bigler ED, et al. Cerebellar atrophy after moderate-to-severe pediatric traumatic brain injury. AJNR Am J Neuroradiol. 2007; 28:537–42. [PubMed: 17353332]

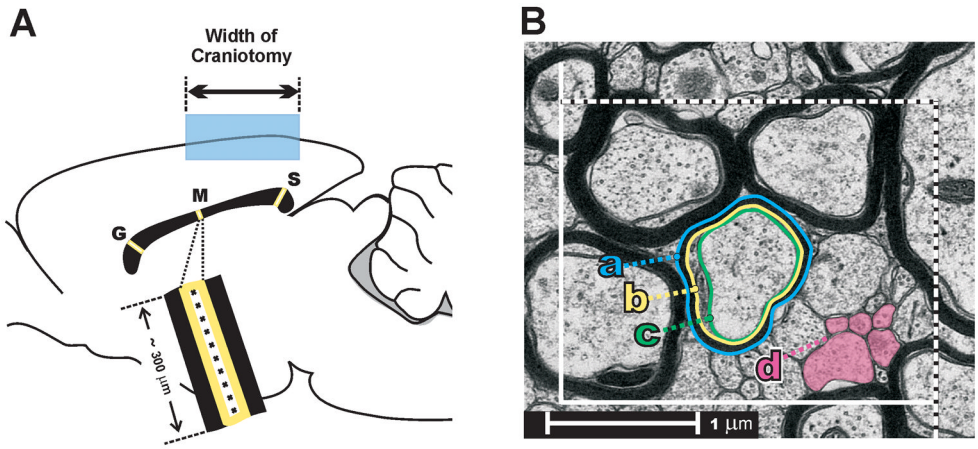

Figure 1.

(**A**) Midsagittal diagram of rat brain, showing sampling scheme covering the dorsal-to-ventral extent of the corpus callosum at genu [G], mid-callosum [M], and splenium [S]. Shaded region shows width and location of craniotomy for midline fluid percussion injury. (**B**) Example of an unbiased stereological counting frame. Shaded profiles [d] show example unmyelinated axon profiles. Representative myelinated profile shows 3 contours that were digitally traced for area measurements: a, outer myelin border; b, inner myelin border; c, axolemma.

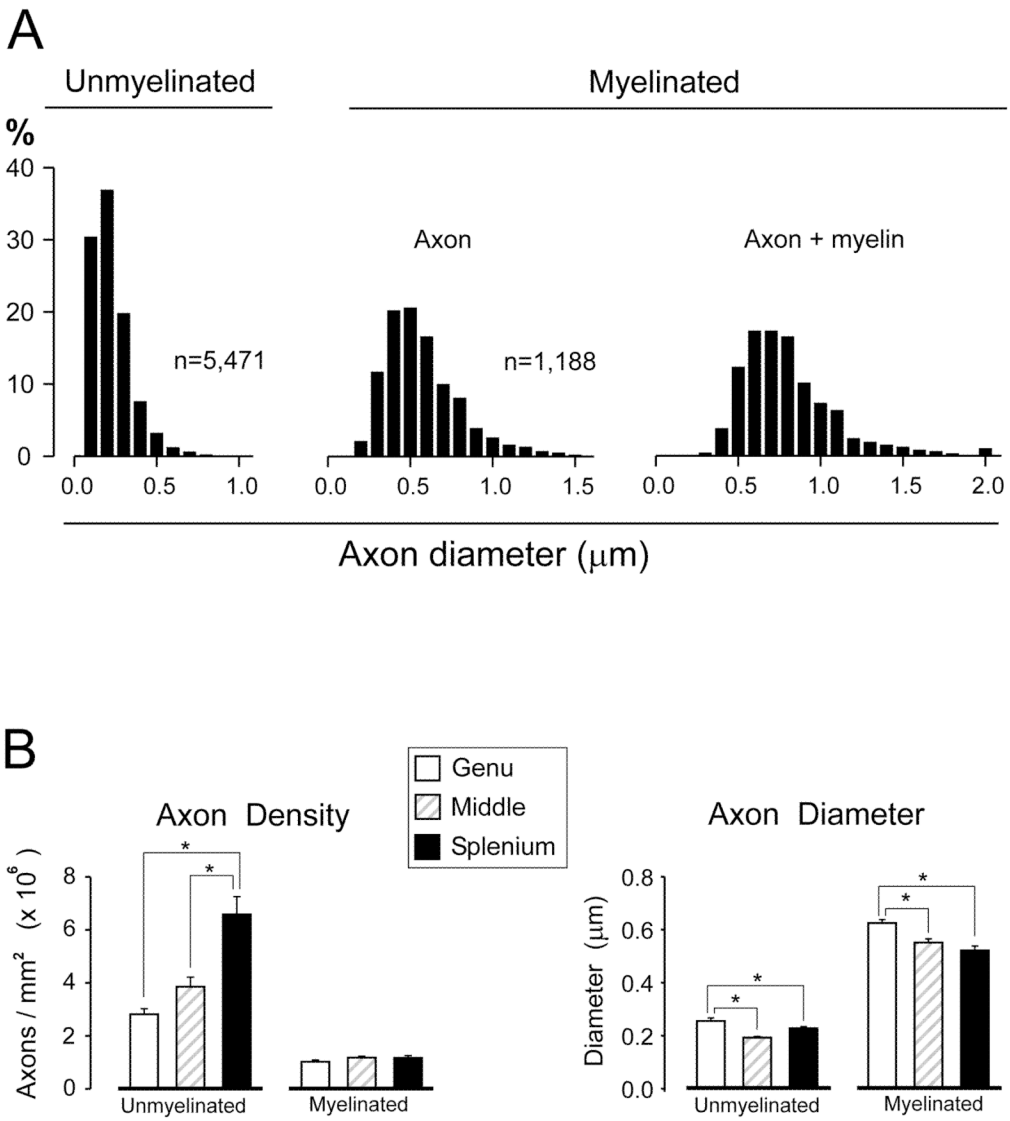

Figure 2.

Characterization of axon populations in sham lesion control rats. (**A**) Distributions of axon diameters for myelinated and unmyelinated axons. Mean diameters and distribution shapes matched prior reports from naïve control rodents (see text), suggesting that the sham lesion procedure did not impact these parameters. (**B**) Separate analyses at callosal regions revealed a rostral-to-caudal (genu-to-splenium) increase in the density of unmyelinated axons, but no gradient for myelinated axons (left panel). Mean axon diameter was significantly greater in the genu than in either posterior region (right panel). *$p < 0.05$.

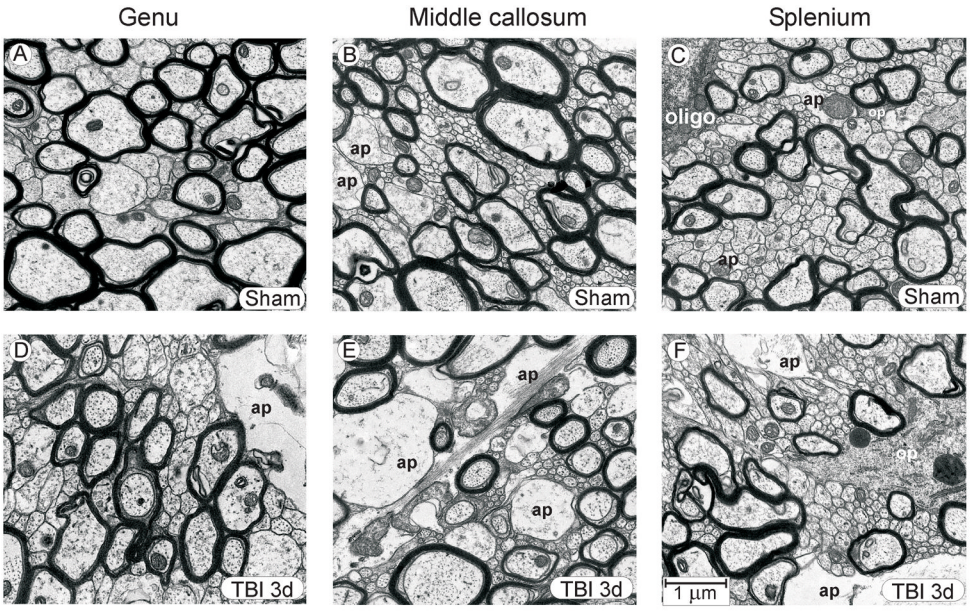

Figure 3.

Representative micrographs, showing genu, mid-callosum, and splenium regions in sham injured control rats (**A–C**) and during the post-injury period when fluid percussion injury-induced change in the unmyelinated axons was well developed (3 days post-injury) (**D–F**). Even though quantitative analyses revealed significant morphometric changes to axonal dimensions at 3 days post-injury, the general architecture of injured tissue was similar to that in sham control tissue, although in some injured rats astrocyte processes were larger and more frequently encountered. The rostral-to-caudal increase in unmyelinated axon density, noted in sham control rats, is preserved in the post-injury samples. Abbreviations: ap, astrocyte process; oligo, oligodendrocyte cell body; op, oligodendrocyte process. Calibration bar in F applies to all panels.

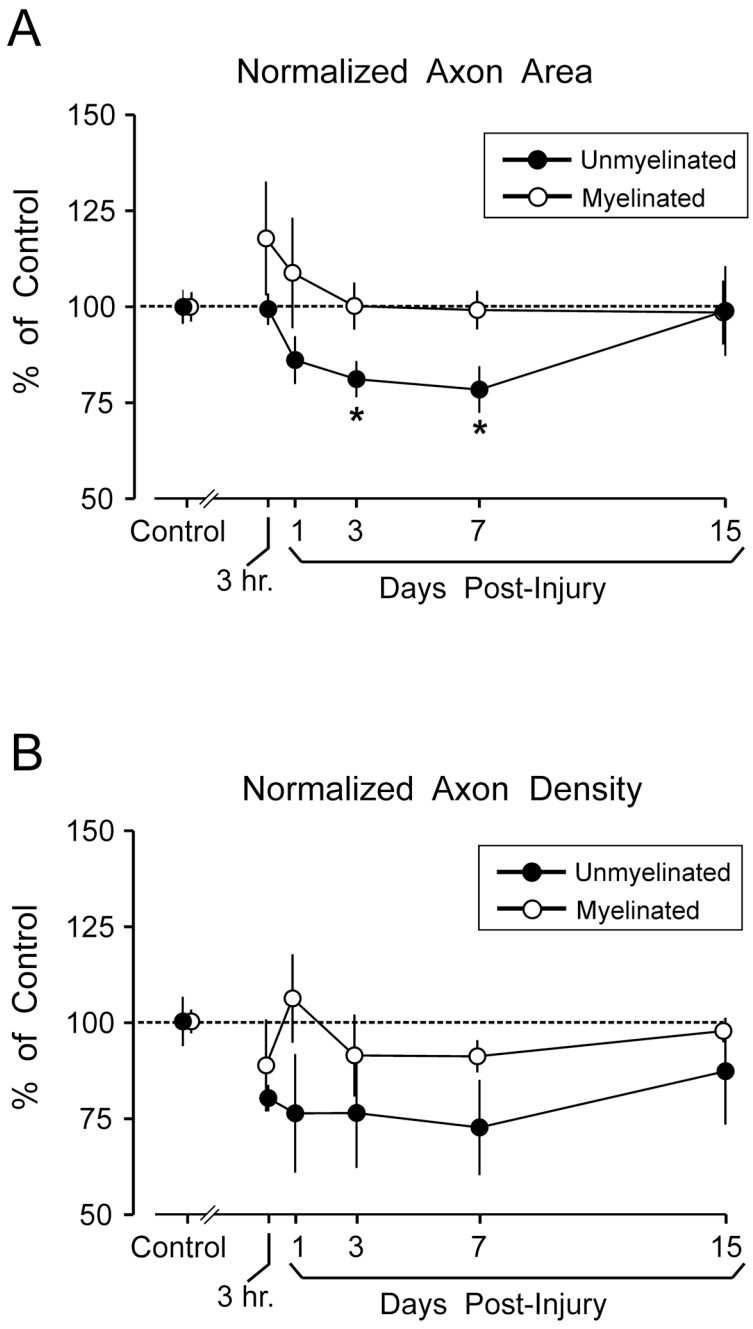

Figure 4.

Effect of moderate fluid percussion injury (FPI) on cross-sectional area of axons and axon density. (**A**) Mean cross-sectional area of axons, averaged across all callosal regions (genu, mid-callosum, and splenium). Results are normalized to the mean axonal area measured in sham injured control rats. Time-dependent axonal shrinkage of unmyelinated fibers was significant (*$p < 0.05$) at 3 days and 7 days post-injury, but recovered to control levels by 15 days. FPI did not significantly alter cross-sectional areas of myelinated axons. (**B**) Mean normalized axon density, averaged across all callosal regions. FPI effects on axonal density were more variable, and reductions in unmyelinated fiber density did not reach significance

at any single survival interval. FPI did not significantly alter density of myelinated axons. Data points in **A** and **B** are slightly offset to avoid overlap of error bars.

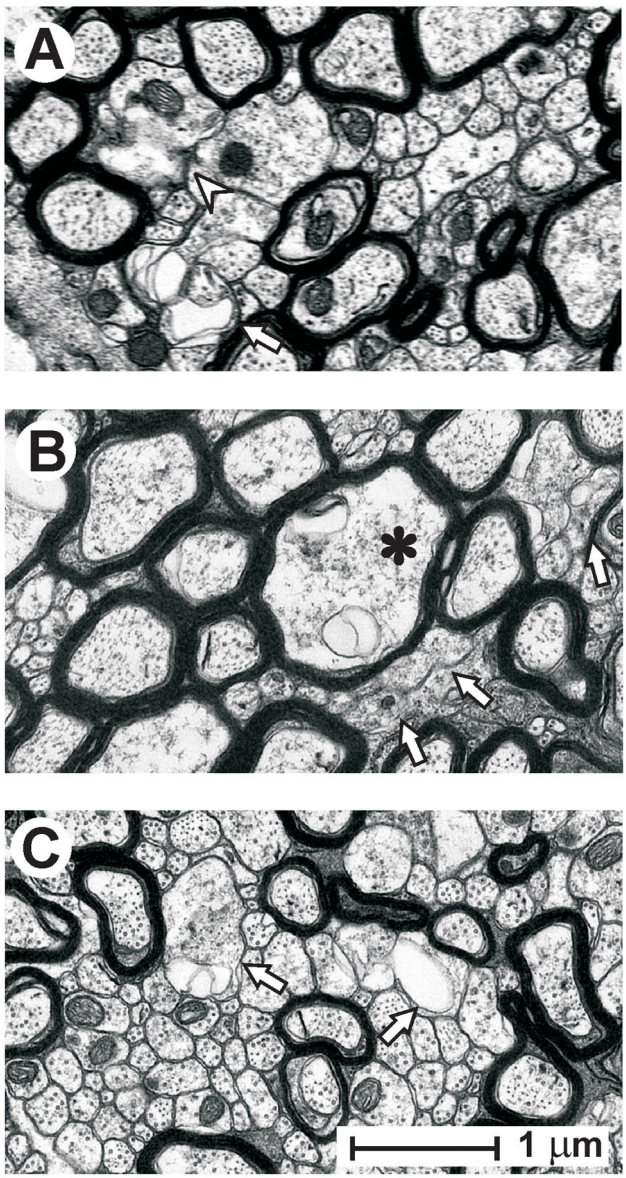

Figure 5.
Representative axonal profiles that failed to meet the operational definition of ‘intact’ in the splenium at 3 days post-injury. (**A**) Isolated unmyelinated axons exhibiting membrane discontinuities (arrowhead) and membranous folding apposed to aberrant extracellular spaces (arrow). (**B**) Clusters of unmyelinated fibers lacking distinct membranes (arrows), along with a myelinated axon (asterisk) with cytoplasmic abnormalities. (**C**) Example of vulnerability of relatively large unmyelinated axons (arrows) juxtaposed to intact small unmyelinated axons. All calibration as in panel **C**.

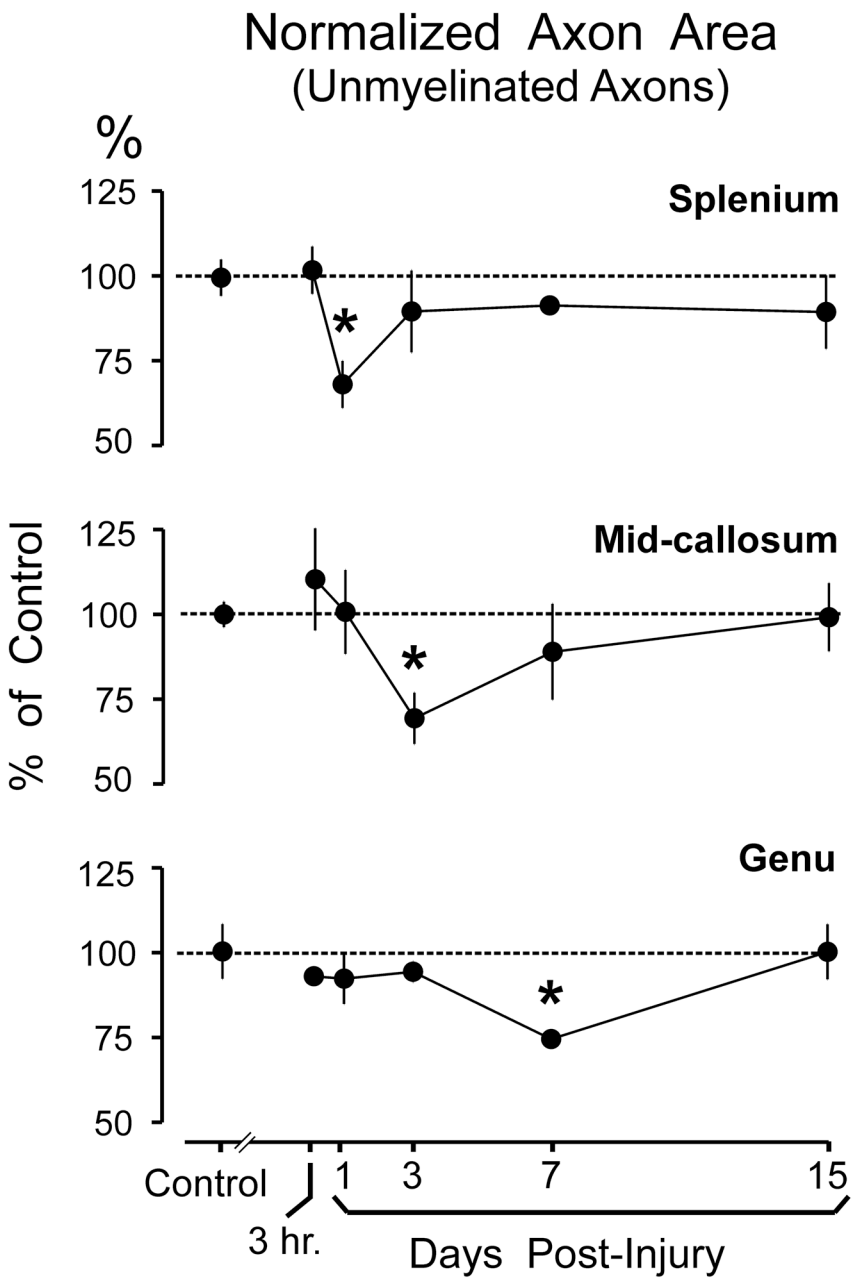

Figure 6.
Effect of moderate fluid percussion injury (FPI) on cross-sectional area of unmyelinated axons in the splenium, middle, and genu regions of the corpus callosum. Results are normalized to the mean axonal area measured in sham injured control rats. FPI produced a caudal-to-rostral sequence of significant axonal shrinkage expressed at 1 day in the splenium, 3 days in the mid-callosum, and 7 days in the genu. Each region showed a recovery to sham control levels following the shrinkage. *$p < 0.05$.

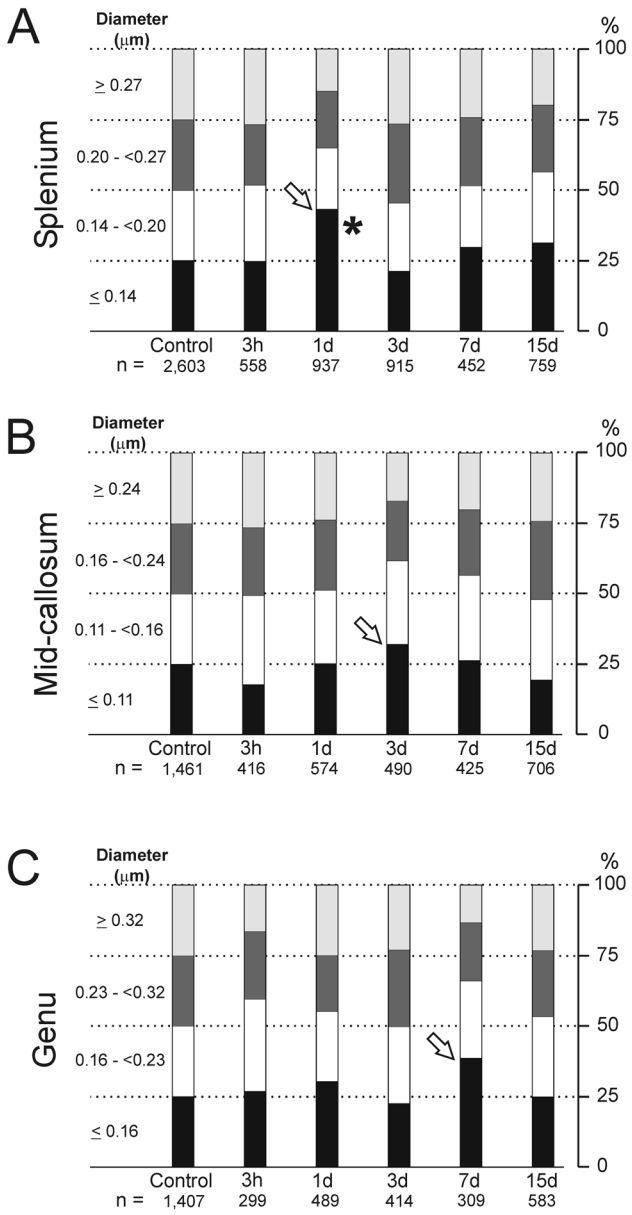

Figure 7.

Fluid percussion injury (FPI) effects on quartile distribution of unmyelinated axon diameters. Quartile values were calculated for the diameters of unmyelinated axons in sham injured control rats (first column), for splenium (**A**), mid-callosum (**B**), and genu (**C**). Columns track post-injury changes over time in the percentage of axons falling in each range. Decreases in the largest quartile coincided with increases in bottom quartile at 1 day (splenium), 3 days (mid-callosum) and 7 day (genu) (arrows), a temporal pattern matching maximum reductions in unmyelinated fiber cross-section areas. Post-injury increases in the lowest quartile were only significant for the splenium (*$p < 0.05$).

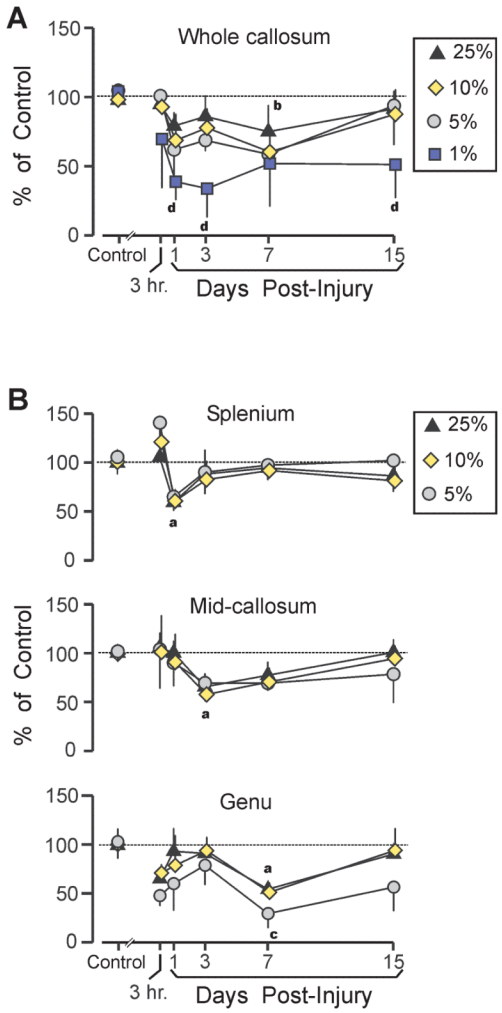

Figure 8.

Effects of traumatic brain injury (TBI) on density of largest intact unmyelinated axons. (**A**) Following fluid percussion injury (FPI), the mean density of the largest 25%, 10%, and 5% diameter intact fibers, combined across all callosal regions, was below sham control levels (significant for top 10% fibers at 7 day), but showed a trend toward a recovery by 15 days. In contrast, the density of the largest 1% fiber category was significantly decreased at 1 day, 3 days, and 15 days. (**B**) Density changes in largest unmyelinated fibers, showed a caudal-to-rostral sequence spanning 1 day to 7 days, similar to post-injury diameter changes (Fig. 6). The largest 5% fiber category was significantly below control levels only in the genu at 7 days. Sham vs. TBI comparisons (all $p < 0.05$): largest 25% ‘a’, 10% ‘b’, 5% ‘c’, 1% ‘d’.

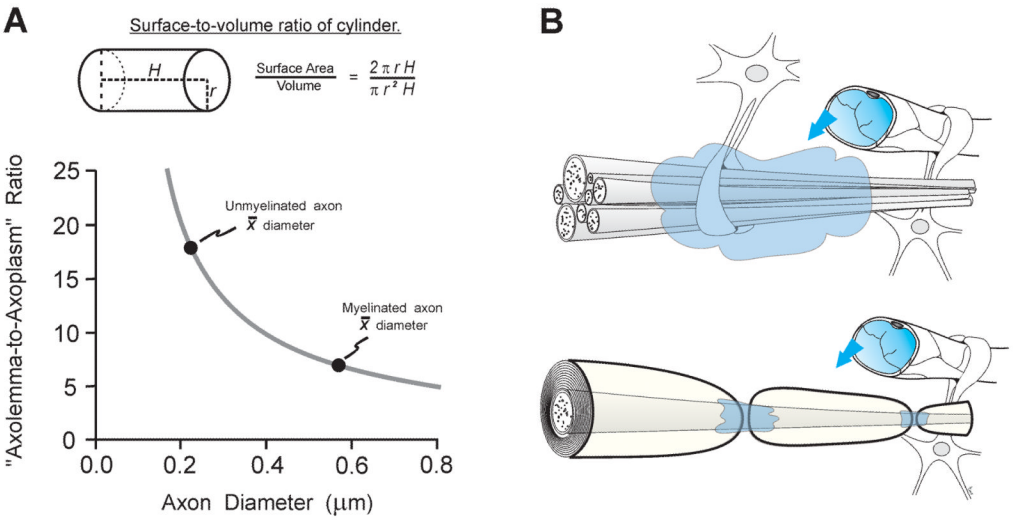

Figure 9.

Morphological properties of unmyelinated axons may place them at elevated risk to traumatic brain injury (TBI). (**A**) Modeling axons as uniform cylinders of arbitrary length, a decrease in diameter corresponds to an increase in surface-to-volume ratio (upper panel). This increased ratio of axolemma area to axoplasm volume probably constitutes a risk to membrane-targeting pathogenetic mechanisms. Mean diameters for unmyelinated and myelinated axons measured in the present study are plotted on the curve-relating diameter to the surface-to-volume ratio (lower panel). The mean diameter of unmyelinated axons is about 60% smaller than the mean myelinated diameter, but this corresponds to an approximate 160% increase in the surface-to-volume ratio. (**B**) Diagram of unmyelinated axons and a myelinated axon in relation to non-neuronal elements (blood vessels, astrocytes). Unmyelinated axolemma is more exposed than myelinated axolemma to destructive extracellular influences (shading) arising locally (e.g. ionic imbalances and activated proteases) or from blood-borne factors penetrating through a compromised blood-brain barrier (arrows). These structural differences likely contribute to a greater vulnerability of unmyelinated axons in some injury conditions.